Available online at www.sciencedirect.com
ScienceDirect
International Journal of Heat and Mass Transfer 51 (2008) 736–746
International Journal of HEAT and MASS TRANSFER
www.elsevier.com/locate/ijhmt

Effect of wall proximity in fluid flow and heat transfer from a rectangular prism placed inside a wind tunnel

Dipes Chakrabarty [a,*], Ranajit Kumar Brahma [b,1]

[a] MCKV Institute of Engineering, Department of Automobile Engineering, Liluah 711 204, West Bengal, India
[b] Indian Institute of Technology, Department of Mechanical Engineering, Kharagpur 721 302, West Bengal, India

Received 22 March 2006
Available online 17 July 2007

Abstract

Experimental investigations in fluid flow and heat transfer have been carried out to study the effect of wall proximity due to flow separation around rectangular prisms. Experiments have been carried out for the Reynolds number 4.9×10^4, blockage ratios are 0.1, 0.2, 0.3 and 0.4, aspect ratio (d/c) are 1.5, 1.33, 0.667 and 0.333, different height-ratios and various angles of attack. The static pressure distribution has been measured on all faces of the rectangular prisms. The results have been presented in the form of pressure coefficient, drag coefficient for various height-ratios and blockage ratios. The pressure distribution shows positive values on the front face whereas on the rear face negative values of the pressure coefficient have been observed. The positive pressure coefficient for different height-ratios does not vary too much but the negative values of pressure coefficient are higher for all points on the surface as the bluff body approaches the upper wall of the wind tunnel. The drag coefficient decreases with the increase in angle of attack as the height-ratio decreases. There is no definite angle of attack for all blockage ratios and Reynolds numbers at which the value of drag coefficient is either maximum or minimum. The heat transfer experiments have been carried out under constant heat flux condition. Heat transfer coefficient are determined from the measured wall temperature and ambient temperature and presented in the form of Nusselt number. Both local and average Nusselt numbers have been presented for various height-ratios. The variation of local Nusselt number has been shown with non-dimensional distance for different angles of attack and blockage ratios. The variation of average Nusselt number has also been shown with different angles of attack for blockage ratios. The local as well as average Nusselt number decreases as the height-ratio decreases for all non-dimensional distance and angle of attack, respectively, for rectangular prisms. The average Nusselt number for rectangular prisms of different blockage ratio varies with the angle of attack. But there is no definite angle of attack at different blockage ratio at which the value of average Nusselt number is either maximum or minimum. Empirical correlations for average Nusselt number have been presented for rectangular prism as a function of Reynolds number, Prandtl number and relevant non-dimensional parameters.

Keywords: Flow separation; Rectangular prism; Blockage ratio; Height-ratio; Angle of attack; Pressure coefficient; Drag coefficient; Nusselt number

1. Introduction

Many investigations have been carried out for heat transfer by forced convection between the exterior surface of bluff bodies such as spheres, cylinder, and square, triangular and rectangular prisms. The important characteristics of flow over a bluff body lie in the nature of the boundary layer. As the streamlines pass over a bluff body, separation takes place due to excessive loss of momentum at adverse pressure gradient from a point, which is not far from the leading edge of the bluff body. The study of heat transfer from a bluff body is important in number of fields such as heat exchanger, gas turbine blades, hot wire anemometry and cooling of electronic equipments.

By extensive search of the literature it is revealed that fluid flow over different shaped bluff bodies like square,

* Corresponding author. Tel.: +91 9433159635.
E-mail addresses: dipes_chak@yahoo.co.in (D. Chakrabarty), rkbrahma@mech.iitkgp.ernet.in (R.K. Brahma).
[1] Tel.: +91 3222 282908.

0017-9310/$ - see front matter © 2007 Elsevier Ltd. All rights reserved.
doi:10.1016/j.ijheatmasstransfer.2007.04.039

Nomenclature

A	surface area of the bluff body, m^2
A_h	heating foil surface area, m^2
c	side length of the rectangular prism, mm
c/H	blockage ratio of the rectangular prism, a non-dimensional number
C_D	drag coefficient $= F_D/(0.5\rho_a u^2 A)$
C_p	pressure coefficient $= (p - p_a)/(0.5\rho_a u^2)$
d	breadth of the rectangular prism, mm
d/c	aspect ratio of the rectangular prism, a non-dimensional number
F_D	drag force, N
h_x	local heat transfer coefficient, W/m^2 K
h_a	average heat transfer coefficient, W/m^2 K
H	height of the wind tunnel, mm
I	current, amp
k	thermal conductivity, W/m K
Nu_x	local Nusselt number $(h_x c/k)$
Nu_a	average Nusselt number $(h_a c/k)$
p	static pressure, mm of water
p_a	ambient pressure, mm of water
Pr	Prandtl number
q	heat flux, W/m^2
Re	Reynolds number based on the velocity of air and the characteristics length of the bluff body $= (uc/v_a)$
T_a	ambient temperature, K
T_x	local wall temperature, K
ΔT	difference between local wall temperature and ambient temperature, K
u	velocity of air, m/s
V	voltage, volts
w	uncertainty
x	distance from the edge of the prism, mm
x/c	non-dimensional distance for the rectangular prism
y	distance of the centroid of the bluff body from the upper wall of the wind tunnel
y/H	height-ratio, a non-dimensional number
α	angle of attack, °
β	coefficient of thermal expansion, K^{-1}
ρ_a	density of air, kg/m^3
ρ_w	density of water, kg/m^3
μ_a	dynamic viscosity of air, N s/m^2
v_a	kinematic viscosity of air, m^2/s

triangular, circular, rectangular and toroids has been investigated thoroughly [1–13]. Lyn et al. [10] studied the turbulent shear layer and the associated recirculation region on the sidewall formed in flow separation from the forward corner of a square cylinder with one opponent laser Doppler velocimetry. Because of vortex shedding, the flow is approximately periodic, and is treated as separated flow undergoing large amplitude forcing at the shedding frequency. Biswas et al. [13] have been studied numerically about the flow past a square cylinder using large-eddy simulations technique and found that there are in good agreement with the experimental results in the time and span averaged axial and transverse velocities in the downstream of the cylinder. The literatures are also available for heat transfer from different geometric shaped bluff bodies at various conditions like various angles of attack and Reynolds numbers [14–24]. From the various literatures it appears that the experimental investigations on fluid flow and heat transfer studies considering the wall effect (i.e. by varying the distance from the wall) with different angles of attack as well as different locations on rectangular prisms have not been adequately covered. In the present work, experimental investigations are carried out to determine the pressure and drag coefficients from the measurement of the pressure distributions around the rectangular prisms and the average heat transfer rates of the prism as influenced by (i) Reynolds number, (ii) angle of attack, (iii) blockage ratio and (iv) ratio of the distance of the centroid of the bluff body from the upper wall to the height of the test section in the wind tunnel.

2. Experimental technique

The schematic diagram and the photographic view of the experimental set-up are shown in Figs. 1 and 2, respectively. The photographic view of the model of rectangular prisms for measurement of static pressure distribution and heat transfer are shown in Figs. 3 and 4, respectively. The experimental set-up consists of wind tunnel driven by an axial flow fan, the model within the test section of the wind tunnel. The experiment has been carried out in a low speed wind tunnel with a working section 300 mm high, 150 mm wide and 800 mm long. The test model has been fitted along the width of the test section. There is a

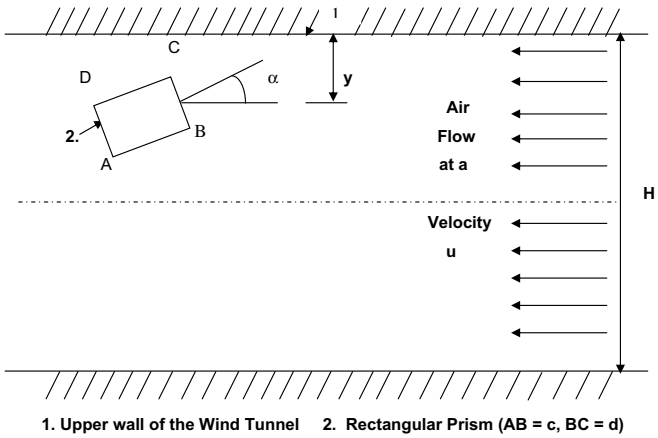

Fig. 1. Schematic diagram of the experimental set up.

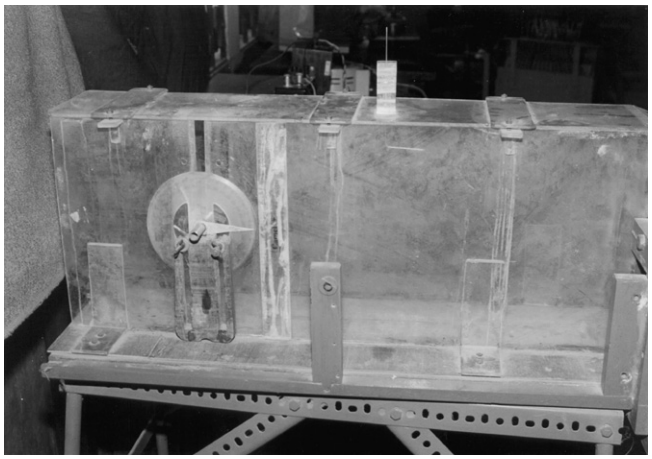

Fig. 2. Photographic view of the experimental set up.

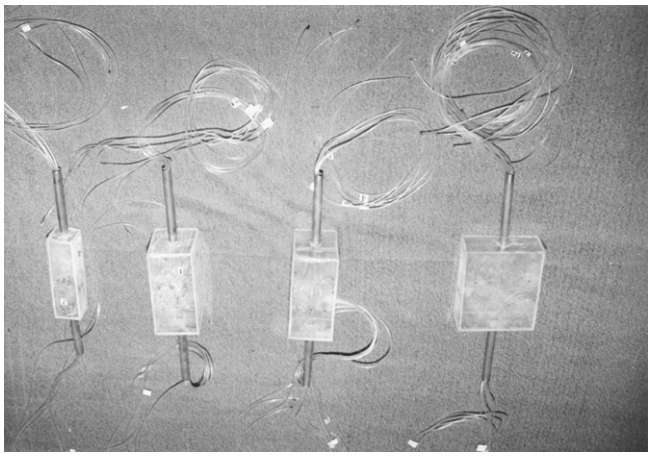

Fig. 3. Photographic view of the models of rectangular prism for measurement of static pressure distribution.

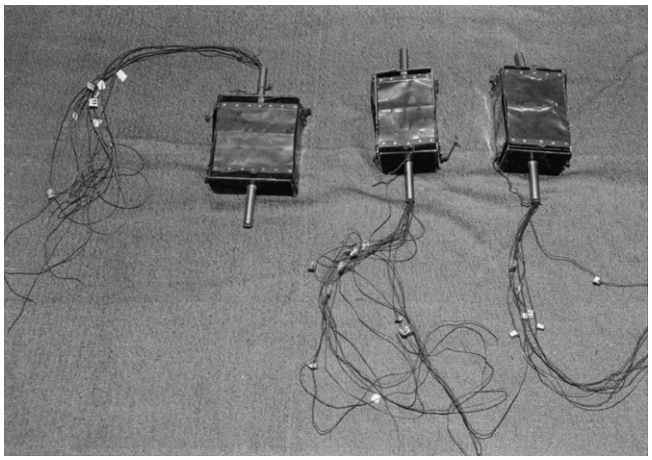

Fig. 4. Photographic view of the models of rectangular prism used for measurement of heat transfer.

slotting arrangement along the sidewall of test section of the wind tunnel for lifting the bluff body from the center towards the upper wall of the wind tunnel to investigate the wall effect on fluid flow and heat transfer characteristics. A pitot tube has measured the approach velocity of the undistributed flow. The pitot tube has been placed inside the wind tunnel facing the direction of airflow. A protractor is attached with the bluff body and is fitted at the side wall of the wind tunnel to measure the angle of rotation of the bluff body by a hollow mild steel pipe from the extension of the inside of the bluff body. The rectangular prisms are made of perspex sheet of 2.5 mm thickness. The sides of the prisms are 30 mm × 45 mm, 60 mm × 80 mm, 90 mm × 60 mm and 120 mm × 40 mm and the length of the prisms are 140 mm. Two pressure tapings on 30 mm side and three pressure tapings on 45 mm side, each of 1 mm diameter are provided of 30 mm × 45 mm side prism. The position of the holes are 10, 20 mm $(x/c = 0.333, 0.667)$ on 30 mm side and 10, 25, 35 mm $(x/c = 0.333, 0.833, 1.167)$ on 45 mm side. Three pressure tapings are provided on the centerline of all the faces of 60 mm × 80 mm side prism. The position of the holes are 10, 30, 50 mm $(x/c = 0.167, 0.5, 0.833)$ on 60 mm side and 20, 40, 60 mm $(x/c = 0.25, 0.5, 0.75)$ on 80 mm side and same numbers of pressure tapings are provided of all the faces of 90 mm × 60 mm side prism. The position of the holes are 25, 45, 65 mm $(x/c = 0.278, 0.5, 0.722)$ on 90 mm side and 10, 30, 50 mm $(x/c = 0.111, 0.333, 0.556)$ on 60 mm side. Five pressure tapings on 120 mm side and three pressure tapings on 40 mm side are provided of 120 mm × 40 mm side prism. The positions of the holes are 20, 40, 60, 80, 100 mm $(x/c = 0.167, 0.333, 0.5, 0.667, 0.833)$ on 120 mm side and 5, 20, 35 mm $(x/c = 0.0417, 0.167, 0.2917)$ on 40 mm side. Stainless steel tubes of 1 mm outside diameters are fitted in these tapping and they are connected to a multitube manometer by flexible tubes for measurement of static pressure distribution. The measurements are taken for the following parameters: (a) angle of attack $(\alpha) = 0$–85°, (b) blockage ratio $(c/H) = 0.1, 0.2, 0.3$ and 0.4, (c) height ratio $(y/H) = 0.5$, 0.350, 0.267, 0.217 and 0.167, (d) Reynolds numbers $= 4.9 \times 10^4$, and (e) aspect Ratio (d/c): 1.5, 1.33, 0.667 and 0.333.

The heat transfer experiment has been done under constant heat flux condition. Constant heat flux condition has been maintained by supplying electrical power to the heating foils. The bodies are made of bakelite. Sufficient insulation has been provided to minimize the heat loss. Stainless steel foils of 0.03 mm thickness have been used for the purpose of producing constant heat flux. The foils are polished to minimize the heat loss due to radiation. The foils are connected with copper strip on both sides through which the power is supplied. The purpose of the present investigation is to measure the local wall temperature distribution at steady state condition by thermocouples at different points for calculation of local as well as average heat transfer coefficient and Nusselt number. Two thermocouples on 30 mm side and three thermocouples on 45 mm side are embedded on rectangular prism of 30 mm × 45 mm side prism. The position of the thermocouples are 10, 20 mm

$(x/c = 0.333, 0.667)$ on 30 mm side and 5, 20, 35 mm $(x/c = 0.167, 0.667, 1.167)$ on 45 mm side. Three thermocouples are embedded on all the faces of 60 mm × 80 mm side prism. The position of the thermocouples are 20, 30, 40 mm $(x/c = 0.333, 0.5, 0.667)$ on 60 mm side and 20, 40, 60 mm $(x/c = 0.333, 0.667, 1)$ on 80 mm side. Three thermocouples on 90 mm side and two thermocouples on 60 mm side are embedded on rectangular prism of 90 mm × 60 mm side prism. The position of the thermocouples are 20, 45, 70 mm $(x/c = 0.222, 0.5, 0.778)$ on 90 mm side and 20, 40 mm $(x/c = 0.222, 0.444)$ on 60 mm side. Four thermocouples on 120 mm side and two thermocouples on 40 mm side are embedded on rectangular prism of 120 mm × 40 mm side prism. The positions of the thermocouples are 15, 45, 75, 105 mm $(x/c = 0.125, 0.375, 0.625, 0.875)$ on 120 mm side and 15, 25 mm $(x/c = 0.125, 0.2083)$ on 40 mm side. The thermocouple beads are soldered at the relevant points on the stainless steel foils. The thermocouple wires are brought out through one end-side of the prism and connected to a digital micro-voltmeters via a selector switch. There is an arrangement for giving power supply to different faces of the prism through a variac so that the experiment can be conducted for different heat inputs. In addition, voltmeters and ammeters have measured the voltage drop and current across the stainless steel foils, respectively.

3. Results and discussion

3.1. Fluid flow characteristics

The flow characteristics around a rectangular prism have been studied by measuring the pressure distribution on different faces of the prism. From the results it is observed that the pressure distribution varies with the size of the prism as well as with the position of the bluff body with respect to the upper wall. It has been found that the pressure distribution varies considerably with the angle of attack. As the air flows over the prism, the front faces show positive pressure coefficient and the flow separation occurs at the rear face causing negative pressure coefficient. For determination of pressure coefficient (C_p), the pressure difference $(p - p_a)$ has been non-dimensionalised by dividing with $0.5\rho_a u^2$ of the air. Figs. 5 and 6 show the variation of pressure coefficient on different faces the rectangular prism at different height-ratios (i.e. $y/H = 0.5, 0.350$, 0.217 and 0.167) for angle of attack 0° and 30°, respectively. The experiment has been conducted for $Re = 4.9 \times 10^4$, $c/H = 0.1$ and $d/c = 1.5$. The positive pressure coefficients for all figures are almost of same values for all height-ratios at all points of surface. The negative pressure coefficients increase as the value of height-ratio decreases, i.e. as the prism approaches the upper wall of the wind tunnel and the value of negative pressure coefficients for different height-ratio as a distinct variation. Figs. 7 and 8 show the plot of pressure coefficient on different faces the rectangular prism at different height-ratios (i.e.

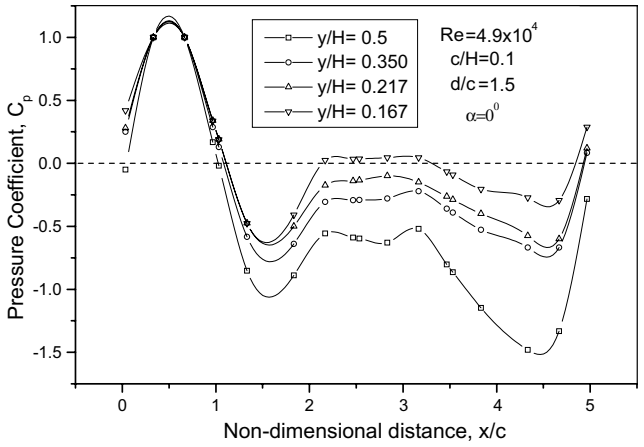

Fig. 5. Variation of pressure coefficient with non-dimensional distance at different height-ratios of a rectangular prism ($c/H = 0.1$, $d/c = 1.5$, $\alpha = 0°$).

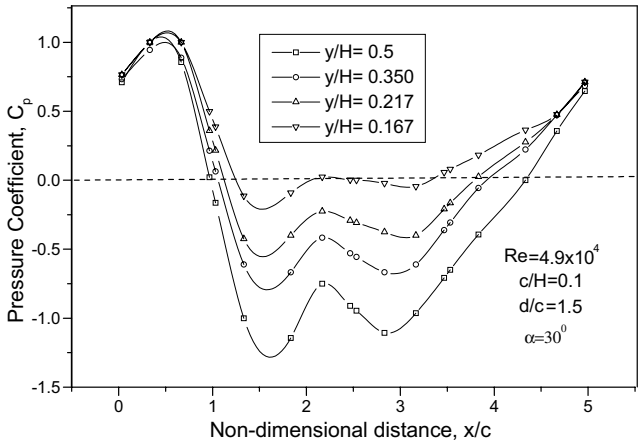

Fig. 6. Variation of pressure coefficient with non-dimensional distance at different height-ratios of a rectangular prism ($c/H = 0.1$, $d/c = 1.5$, $\alpha = 30°$).

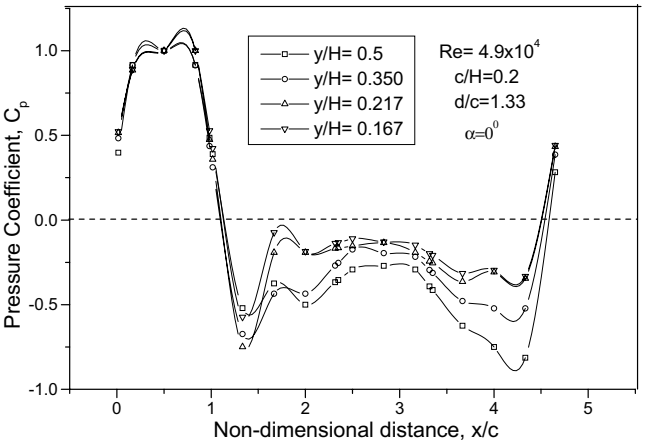

Fig. 7. Variation of pressure coefficient with non-dimensional distance at different height-ratios of a rectangular prism ($c/H = 0.2$, $d/c = 1.33$, $\alpha = 0°$).

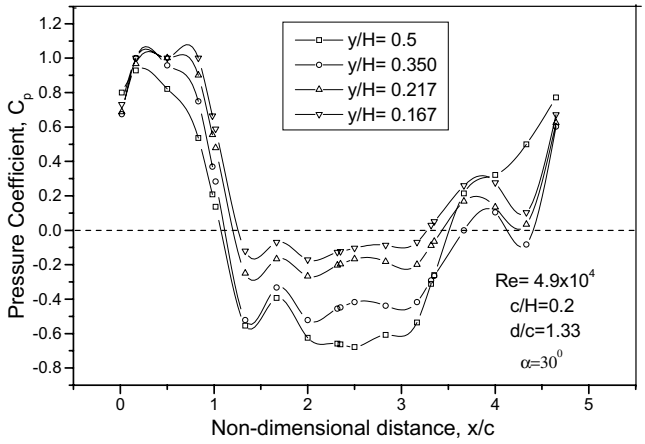

Fig. 8. Variation of pressure coefficient with non-dimensional distance at different height-ratios of a rectangular prism ($c/H = 0.2$, $d/c = 1.33$, $\alpha = 30°$).

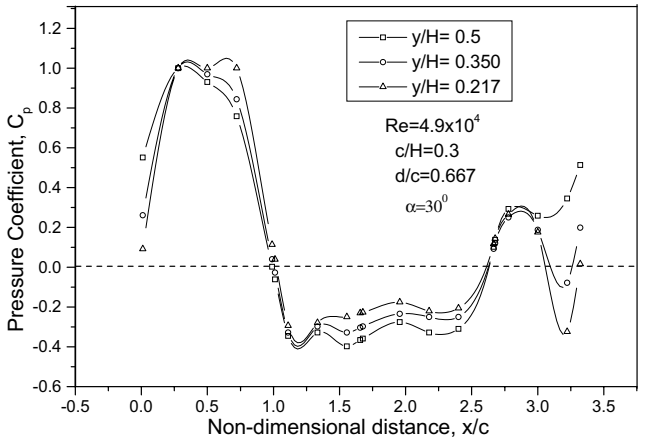

Fig. 10. Variation of pressure coefficient with non-dimensional distance at different height-ratios of a rectangular prism ($c/H = 0.3$, $d/c = 0.67$, $\alpha = 30°$).

$y/H = 0.5, 0.350, 0.217$ and 0.167) for angle of attack 0° and 30°, respectively. The experiment has been conducted for $Re = 4.9 \times 10^4$, $c/H = 0.2$ and $d/c = 1.33$. In Figs. 7 and 8, the negative pressure coefficients are higher at all points (i.e. x/c) as the value of y/H decreases. The positive pressure coefficients are almost same at all points of x/c for all height-ratios in Fig. 7 while in Fig. 8 the positive value of C_p at some points are higher as y/H decreases. Similarly, Figs. 9 and 10 show how the pressure coefficient varies on different faces the rectangular prism at different height-ratios (i.e. $y/H = 0.5, 0.350$ and 0.217) for angle of attack 0° and 30°, respectively. The experiment has been conducted for $Re = 4.9 \times 10^4$, $c/H = 0.3$ and $d/c = 0.667$. The nature of curve of pressure coefficient is nearly same for Figs. 9 and 10. The values of positive pressure coefficient is almost equal at all points of x/c for every y/H while the negative pressure coefficients are higher for lesser value of y/H. The plot of C_p with x/c for $y/H = 0.5, 0.350$ and 0.267 at $Re = 4.9 \times 10^4$, $c/H = 0.4$ and $d/c = 0.33$

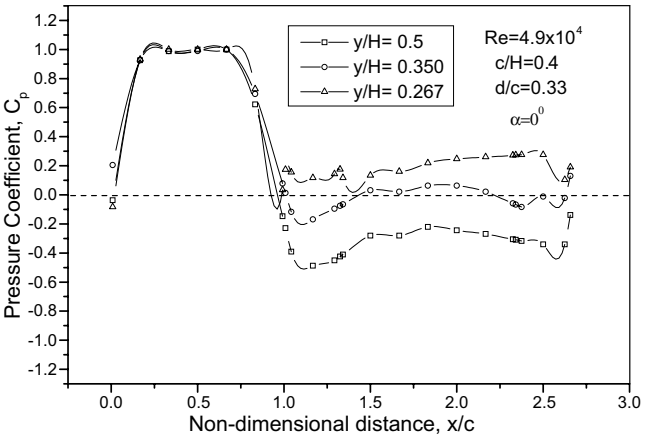

Fig. 11. Variation of pressure coefficient with non-dimensional distance at different height-ratios of a rectangular prism ($c/H = 0.4$, $d/c = 0.33$, $\alpha = 0°$).

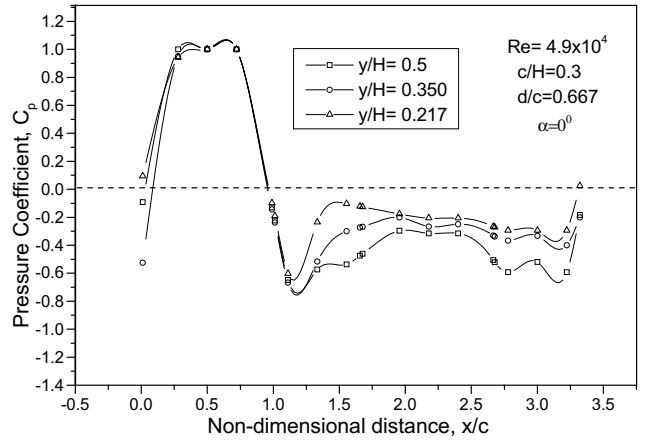

Fig. 9. Variation of pressure coefficient with non-dimensional distance at different height-ratios of a rectangular prism ($c/H = 0.3$, $d/c = 0.67$, $\alpha = 0°$).

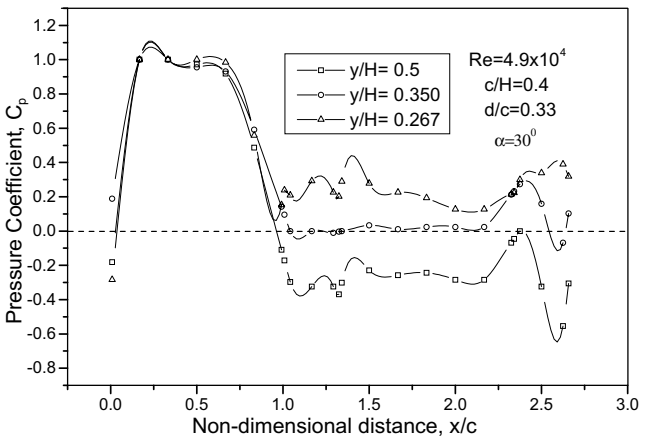

Fig. 12. Variation of pressure coefficient with non-dimensional distance at different height-ratios of a rectangular prism ($c/H = 0.4$, $d/c = 0.33$, $\alpha = 30°$).

are plotted in Figs. 11 and 12 for angle of attack 0° and 30°, respectively. Figs. 11 and 12 show that the positive values of C_p are almost of same value for all y/H. At some points (i.e. x/c) the values of C_p are negative at $y/H = 0.5$ while for the same points the value of pressure coefficients at $y/H = 0.350$ and 0.267 are positive.

Drag force (F_D) has been calculated by integrating the pressure distribution in the direction of airflow on the four faces of the rectangular prism. For calculation of drag coefficient (C_D), the drag force F_D has been divided by $0.5\rho_a u^2 A$, where A is the surface area of the bluff body. The variation of drag coefficient with the angle of attacks for different height-ratios, blockage ratios and Reynolds numbers has been shown from Figs. 13–16. It is concluded from all the figures that the value of drag coefficients continuously decreases for all angle of attack as the value of height-ratio (y/H) decreases. All figures have been plotted for the Reynolds numbers 4.9×10^4. Fig. 13 shows the plot of drag coefficient with angle of attack for the blockage ratio = 0.1 and aspect ratio = 1.5. The value of C_D increases from $\alpha = 0°$ to 60° and then decreases from

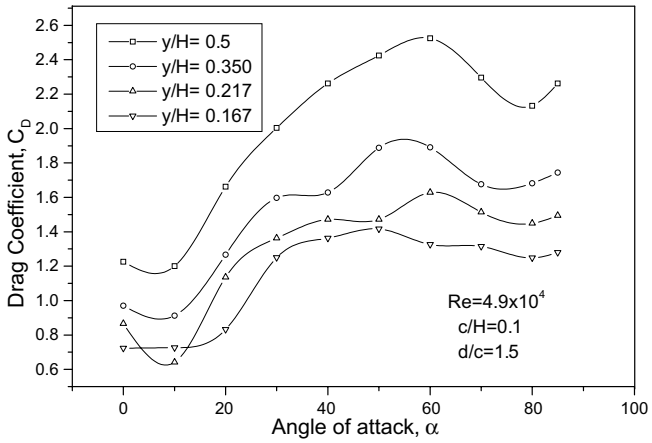

Fig. 13. Variation of drag coefficient with angle of attack at different height-ratios of a rectangular prism ($c/H = 0.1$, $d/c = 1.5$).

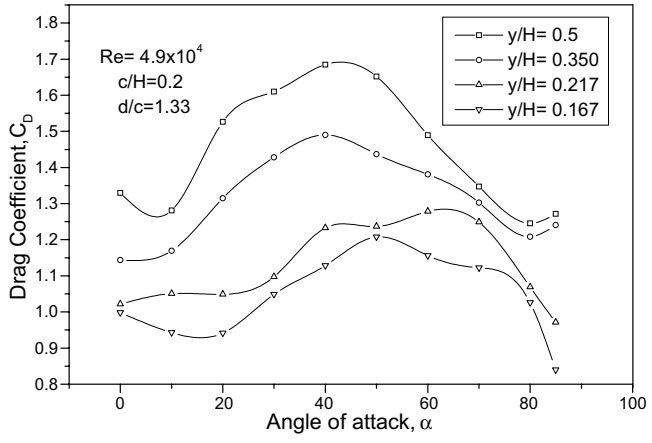

Fig. 14. Variation of drag coefficient with angle of attack at different height-ratios of a rectangular prism ($c/H = 0.2$, $d/c = 1.33$).

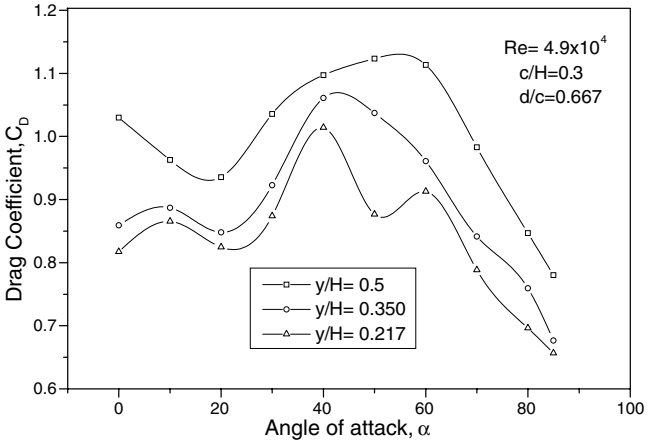

Fig. 15. Variation of drag coefficient with angle of attack at different height-ratios of a rectangular prism ($c/H = 0.3$, $d/c = 0.67$).

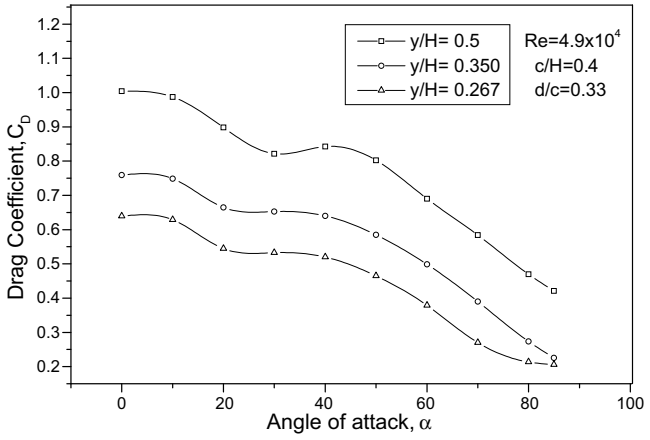

Fig. 16. Variation of drag coefficient with angle of attack at different height-ratios of a rectangular prism ($c/H = 0.4$, $d/c = 0.33$).

$\alpha = 60°$ to 85°. The maximum value of C_D is obtained at the angle of 60° for all height-ratios. In Fig. 14, where $c/H = 0.2$ and $d/c = 1.33$, the value of C_D increases from $\alpha = 10°$ to 40° and then decreases from $\alpha = 40°$ to 85°. The maximum value of C_D is obtained at the angle of 40° for height-ratio = 0.5 and 0.350. The graph between C_D with angle of attack (α) has been plotted in Fig. 15 for $y/H = 0.5, 0.350$ and 0.217. The experiment is performed at $c/H = 0.3$ and $d/c = 0.67$. The maximum value of C_D is obtained at $\alpha = 40°$ for $y/H = 0.350$ and 0.217 while that at $\alpha = 50°$ for $y/H = 0.5$. Fig. 16 shows the variation of drag coefficient with angle of attack for the blockage ratio = 0.4 and aspect ratio = 0.33 and the plot of drag coefficient for all y/H decreases from $\alpha = 0°$ to 30° and again it decreases from $\alpha = 40°$ to 85°.

From the plot between pressure coefficients versus non-dimensional distance, it is observed that as the body approaches the upper wall, the negative pressure coefficient as well as the plot from drag coefficient versus angle of attack, the drag coefficient decreases. It is due to interaction with the boundary layer on the upper wall of the wind

tunnel, the stream line pattern changes and the area under the separation zone at the rear side as well as the upper face of the bluff body (i.e. rectangular prism) decreases.

The uncertainties in Re and C_p have been calculated following the method given by Kline and McClintock [21] and found to be within the range of ±3.8% and ±4.63%, respectively, in this investigation.

3.2. Heat transfer characteristics

Information regarding the heat transfer rate from the bluff bodies are of interest to the designers in engineering practice. In the present investigation, experiments have been conducted for various sizes of the rectangular prisms for generating this information under constant heat flux condition. Heat flux has been calculated from the heat input divided by the surface area of the heating foil. Input heat flux has been corrected by subtracting the heat loss per unit area. Heat loss calculation has been done by using the correlation given by Hossain and Brahma [25]. The side length of the prism has been taken as the characteristics length for the definition of the Nusselt number. Local and average Nusselt numbers have been plotted for various angles of attack, blockage ratios, and height-ratios for different models of rectangular prism. Figs. 17 and 18 show the plot of local Nusselt number with non-dimensional distance for different height-ratios ($y/H = 0.5$, 0.350, 0.217 and 0.167) where $c/H = 0.1$ and $d/c = 1.5$. For all graphs the value of local Nusselt number for all height-ratios changes markedly almost at the point, $x/c = 3.167$. The value of Nu_x does not vary too much for different height-ratios at different points of the surface of the prism. Figs. 19 and 20 show the variation of local Nusselt number with non-dimensional distance for different height-ratios ($y/H = 0.5$, 0.350 and 0.217) at $c/H = 0.2$ and $d/c = 1.33$. For almost all plots the graph of local Nusselt number for all height-ratios changes markedly at $x/c = 1.667$, i.e. the highest value occurs at that point. Figs. 21 and 22

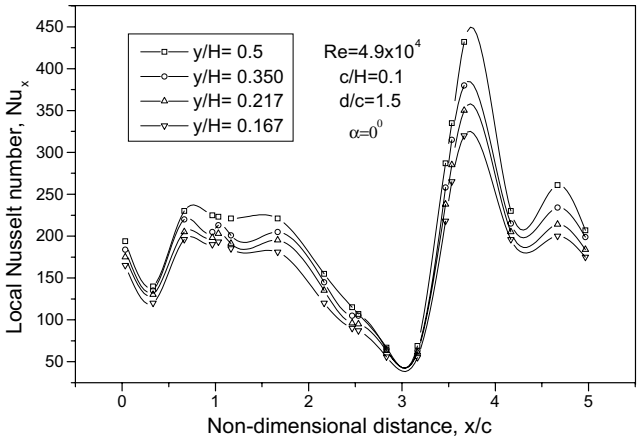

Fig. 17. Variation of local Nusselt number with non-dimensional distance at different height-ratios of a rectangular prism ($c/H = 0.1$, $d/c = 1.5$, $\alpha = 0°$).

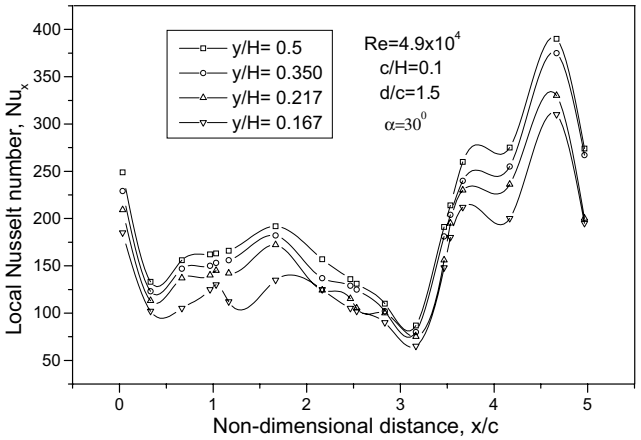

Fig. 18. Variation of local Nusselt number with non-dimensional distance at different height-ratios of a rectangular prism ($c/H = 0.1$, $d/c = 1.5$, $\alpha = 30°$).

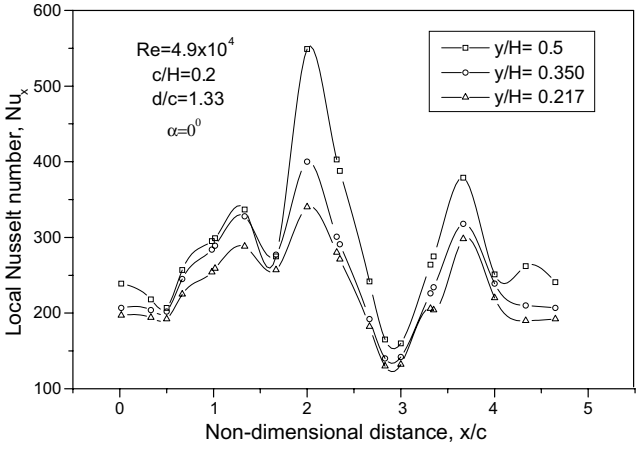

Fig. 19. Variation of local Nusselt number with non-dimensional distance at different height-ratios of a rectangular prism ($c/H = 0.2$, $d/c = 1.33$, $\alpha = 0°$).

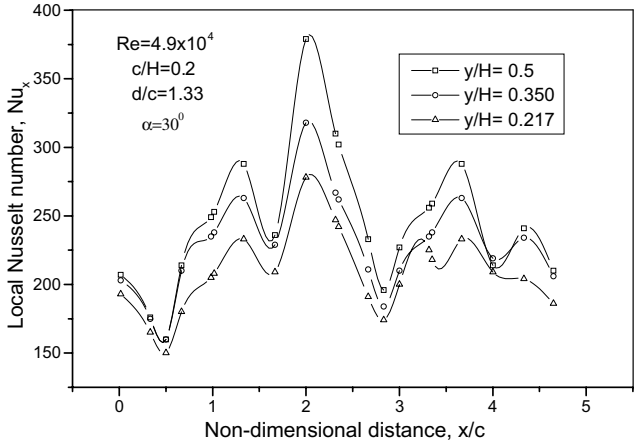

Fig. 20. Variation of local Nusselt number with non-dimensional distance at different height-ratios of a rectangular prism ($c/H = 0.2$, $d/c = 1.33$, $\alpha = 30°$).

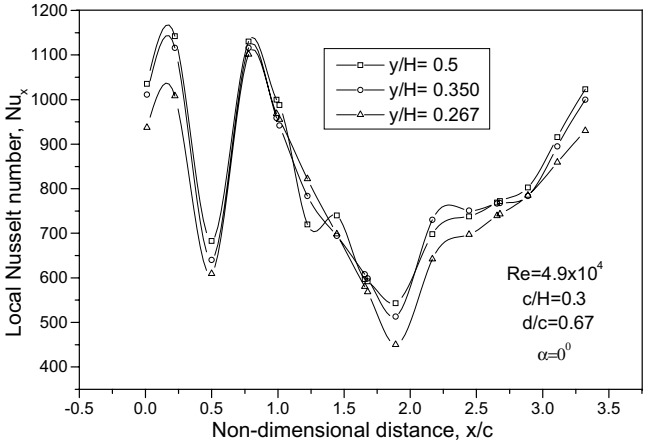

Fig. 21. Variation of local Nusselt number with non-dimensional distance at different height-ratios of a rectangular prism ($c/H = 0.3$, $d/c = 0.67$, $\alpha = 0°$).

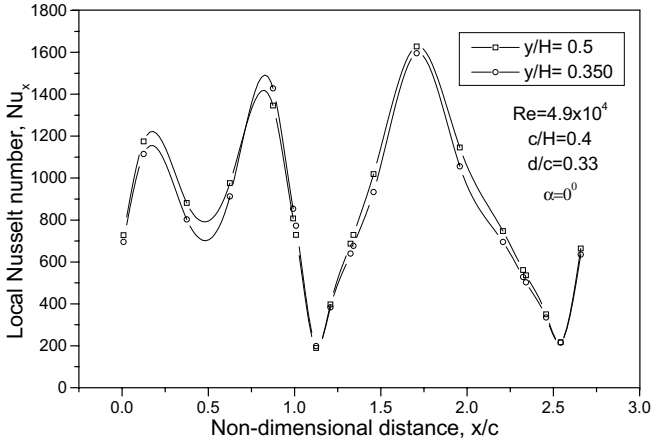

Fig. 23. Variation of local Nusselt number with non-dimensional distance at different height-ratios of a rectangular prism ($c/H = 0.4$, $d/c = 0.33$, $\alpha = 0°$).

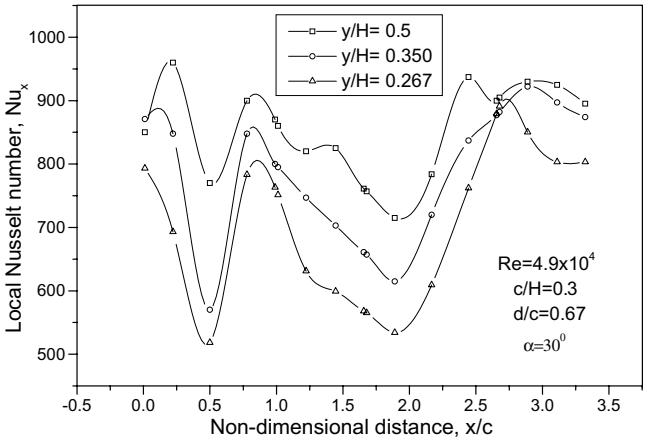

Fig. 22. Variation of local Nusselt number with non-dimensional distance at different height-ratios of a rectangular prism ($c/H = 0.3$, $d/c = 0.67$, $\alpha = 30°$).

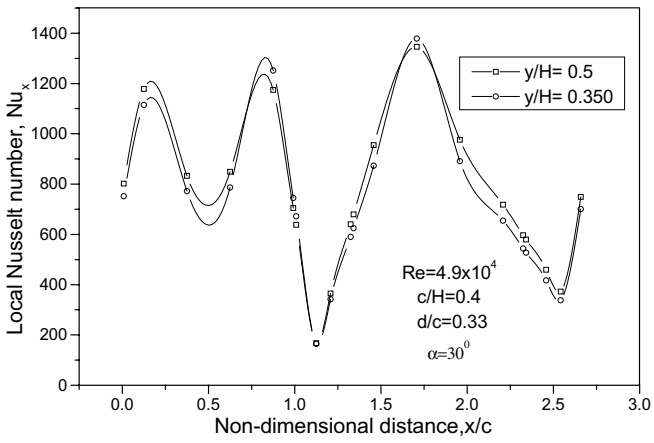

Fig. 24. Variation of local Nusselt number with non-dimensional distance at different height-ratios of a rectangular prism ($c/H = 0.4$, $d/c = 0.33$, $\alpha = 30°$).

show the variation of local Nusselt number with non-dimensional distance for different height-ratios ($y/H = 0.5$, 0.350 and 0.267) at $c/H = 0.3$ and $d/c = 0.67$. In Fig. 21 (i.e. at $\alpha = 0°$), the value of Nu_x for every y/H does not vary too much but in Fig. 22 (i.e. at $\alpha = 30°$) the sharp variation occurs at $x/c = 0.5$, 0.778, 1.889. Figs. 23 and 24 show the plots of local Nusselt number with non-dimensional distance for different height-ratios ($y/H = 0.5$ and 0.350) at $c/H = 0.4$ and $d/c = 0.33$. The plot Nu_x with x/c shows that the values of local Nusselt numbers are higher when the bluff body rests at the centerline of the wind tunnel. The value of local Nusselt number has a sharp variation at various points of x/c for all plots. In Fig. 23, the sharp variation takes place at $x/c = 0.125$, 0.375, 0.875, 1.125, and 1.70833 for all y/H while in Fig. 24, the variation occurs at $x/c = 0.125, 0.875, 1.125,$ and 1.70833.

Average Nusselt numbers have been calculated by this procedure. At first, the value of Nu_x has been integrated for all the four faces separately and then added and divided by 2 (1 + aspect ratio) to get the average value of Nu_a. Average Nusselt numbers have been plotted with the angle of attack for different height-ratios for blockage ratio = 0.1, 0.2, 0.3 and 0.4 at Reynolds number 4.9×10^4. For every plot it is observed that the values of average Nusselt number at every angle of attack decrease as the value of y/H decreases that means the values of Nu_a are less as the prism approaches the upper wall of the wind tunnel. Fig. 25 shows the plot of average Nusselt number with angle of attack for blockage ratio 0.1 and aspect ratio = 1.5 at different y/H (0.5, 0.350, 0.217 and 0.167). The minimum value of Nu_a is observed at $\alpha = 10°$. The variation of Nu_a with α at different height-ratio ($y/H = 0.5$, 0350 and 0.217) are shown for $c/H = 0.2$ and $d/c = 1.33$ in Fig. 26. For this plot, it is observed that the minimum value of Nu_a occurs at an angle of attack is equal to 40°. Fig. 27 shows the variation of Nu_a versus α at $y/H = 0.5$, 0.350 and 0.267 for the blockage ratio = 0.3 and aspect ratio = 0.67. The maximum value of Nu_a is observed at the angle of

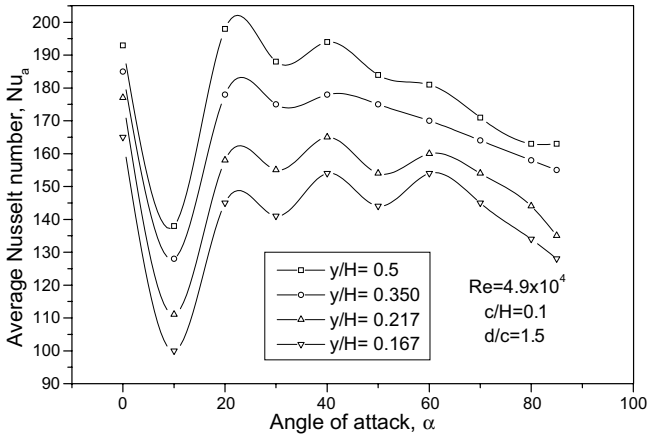

Fig. 25. Variation of average Nusselt number with angle of attack at different height-ratios of a rectangular prism ($c/H = 0.1$, $d/c = 1.5$).

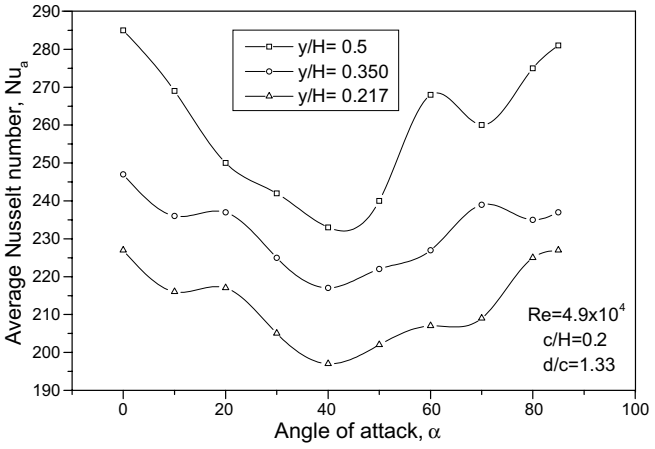

Fig. 26. Variation of average Nusselt number with angle of attack at different height-ratios of a rectangular prism ($c/H = 0.2$, $d/c = 1.33$).

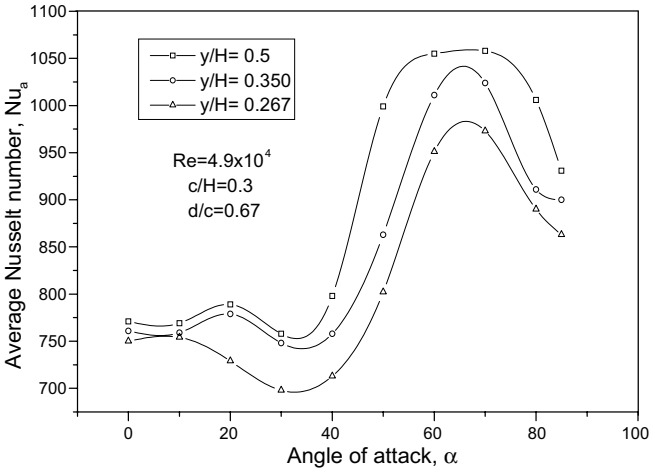

Fig. 27. Variation of average Nusselt number with angle of attack at different height-ratios of a rectangular prism ($c/H = 0.3$, $d/c = 0.67$).

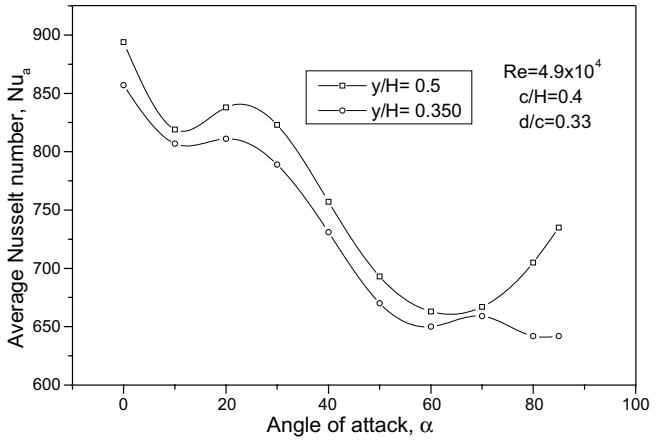

Fig. 28. Variation of average Nusselt number with angle of attack at different height-ratios of a rectangular prism ($c/H = 0.4$, $d/c = 0.33$).

attack is equal to 60°. The plot of Nu_a with α is shown in Fig. 28 where $c/H = 0.4$ and $d/c = 0.33$ and Nu_a decreases from $\alpha = 20°$ to 60° and then again increases.

Regarding the heat transfer experiment, the value of local heat transfer coefficient decreases as the body approaches the upper wall of the wind tunnel as the area under separation zone decreases. But it is really difficult to explain about the characteristics of heat transfer phenomena under flow separation zone. Basically, it depends upon the behavior of the *local fluid mechanics* at that moment.

The uncertainties in local heat transfer coefficient and local Nusselt number have been calculated [26] and found to be within the range of ±4.14% and ±5.45%, respectively.

The average Nusselt number (Nu_a) has been correlated by power function expressions of Reynolds number and other non-dimensional parameters. The coefficients and the exponents of the equation are determined from the experimental results. After calculating the values of the coefficients and the exponents a correlation for Nu_a has been found as follows:

$$\text{(i)}\ Nu_a = 0.43[Re]^{0.65}[Pr]^{0.33}[a/H]^{0.26}[d/c]^{-0.24} \times [y/H]^{0.13}(1-\sin\alpha)^{0.015} \quad \text{(i)}$$

The correlation is valid for the following ranges: $0.1 \leqslant c/H \leqslant 0.2$, $0.167 \leqslant y/H \leqslant 0.5$, $0° \leqslant \alpha \leqslant 85°$ and $0.133 \leqslant d/c \leqslant 1.5$:

$$\text{(ii)}\ Nu_a = 0.67[Re]^{0.55}[Pr]^{0.33}[a/H]^{-1.08}[d/c]^{-0.66} \times [y/H]^{0.05}(1-\sin\alpha)^{-0.70} \quad \text{(ii)}$$

The correlation is valid for the following ranges: $0.3 \leqslant c/H \leqslant 0.4$, $0.167 \leqslant y/H \leqslant 0.5$, $0° \leqslant \alpha \leqslant 85°$, $0.33 \leqslant d/c \leqslant 0.67$.

A comparison has been made between measured and correlated values of Nu_a in Figs. 29 and 30. The experimental measured values of average Nusselt number are within ±4.72% and 5.48% of the correlated values of average Nusselt number.

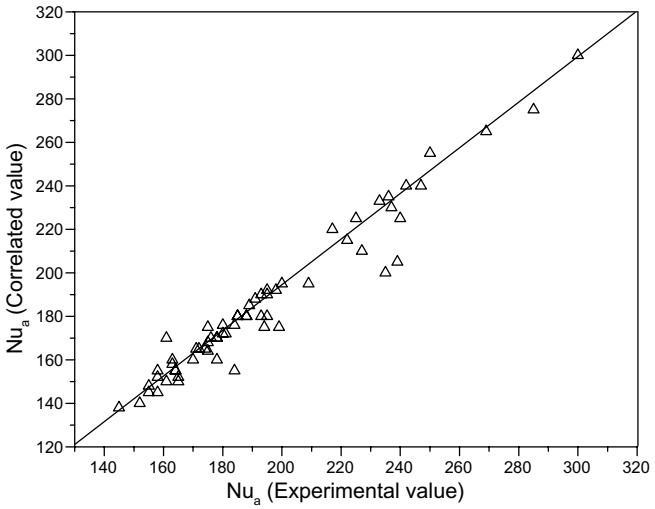

Fig. 29. Comparison of measured and correlate values of average Nusselt number for flow over rectangular prism ($c/H = 0.1$ and 0.2).

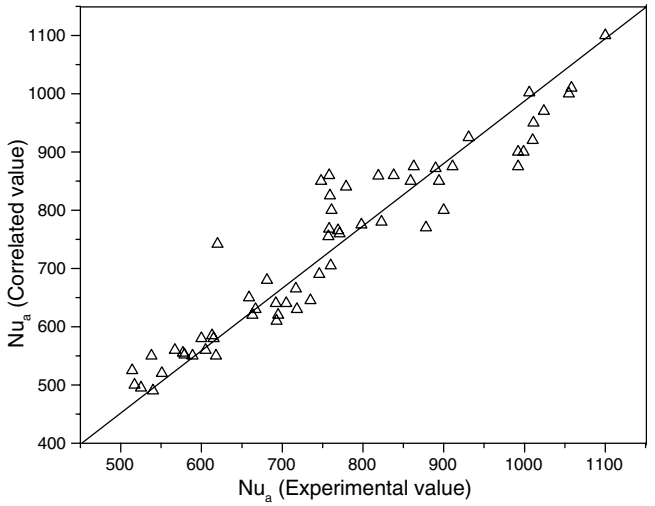

Fig. 30. Comparison of measured and correlate values of average Nusselt number for flow over rectangular prism ($c/H = 0.3$ and 0.4).

4. Conclusions

The following conclusions can be made for rectangular prisms from the results of the experiments:

(i) The pressure coefficient (C_p) shows positive values on the front face whereas the rear face is within the separated flow region for all angles of attack.
(ii) The values of positive pressure coefficients for all blockage ratios are almost at all points on the surface of the prisms at different height-ratios.
(iii) The values of negative pressure coefficients for all blockage ratios and Reynolds numbers increase for almost all points on the surface as the bluff body approaches the upper wall of the wind tunnel.
(iv) The values of drag coefficient (C_D) for all angles of attack, Reynolds numbers and blockage ratios decrease as the prism moves in the direction of the upper wall of the wind tunnel.
(v) There is no definite angle of attack for all blockage ratios and Reynolds numbers at which the value of drag coefficient is either maximum or minimum.
(vi) The local Nusselt number for all blockage ratios decreases as the value of height-ratio decreases for almost all points on the surface as the prism approaches the upper wall of the wind tunnel.
(vii) The values of average Nusselt number (Nu_a) for all angles of attack, Reynolds numbers and blockage ratios decrease as the prism moves in the direction of the upper wall of the wind tunnel.
(viii) There is no definite angle of attack for all blockage ratios and Reynolds numbers at which the value of average Nusselt number is either maximum or minimum.

Acknowledgements

The first author, Dr. Dipes Chakrabarty expresses his deep and sincere sense of indebtedness to Dr. Gautam Biswas, Professor of Department of Mechanical Engineering of I.I.T., Kanpur, for his guidance, help and encouragement in the preparation of this manuscript. Dr. Chakrabarty is also grateful to one of his students of MCKV Institute of Engineering, Liluah of the Department of Automobile Engineering, Miss Arjita Saha Choudhury for her technical help and lots of encouragement.

References

[1] P.W. Bearman, Investigation of flow behind a two dimensional model with blunt trailing edge and fitted with splitter plates, J. Fluid Mech. 21 (Part 2) (1965) 241–255.
[2] P.W. Bearman, D.M. Trueman, An investigation of the flow around rectangular cylinders, Aeronaut. Quart. 23 (1972) 229–237.
[3] C.J. Aplet et al., The effects of wake splitter plates on the flow past a circular cylinder in the range $10^4 < Re < 5 \times 10^4$, J. Fluid Mech. 61 (Part 1) (1973) 187–198.
[4] P.W. Bearman, M.M. Zdravkovich, Flow around a circular cylinder near a plane boundary, J. Fluid Mech. 89 (Part 1) (1978) 53–73.
[5] T. Igarashi, Characteristics of the flow around a square prism, Bull. JSME 27 (231) (1984) 1858–1864.
[6] T. Igarashi, Characteristics of flow around rectangular cylinders, Bull. JSME 28 (242) (1985) 1690–1696.
[7] V. Mansingh, P.H. Oosthuizen, Effects of splitter plates in the wake flow behind a bluff body, AIAA J. (1990) 778–783.
[8] R.L. Simpson, The structure of the near wall region of two dimensional turbulent separated flow, Phils. Trans. Roy. Soc. Lond. 336 (1991) 5–17.
[9] D.A. Lyn et al., A laser – Doppler velocimetry study of ensemble – averaged characteristics of the turbulent near wake of a square cylinder, J. Fluid Mech. 304 (1995) 285–319.
[10] D.A. Lyn, W. Rodi, The flapping shear layer formed by flow separation from the forward corner of a square cylinder, J. Fluid Mech. 267 (1995) 353–376.

[11] A.K. Saha, G. Biswas, K. Muralidhar, Three dimensional study of flow past a square cylinder at low Reynolds number, Int. J. Heat Mass Transfer 24 (2003) 54–66.
[12] S.C. Luo et al., Characteristics of square cylinder wake transition flows, Phys. Fluids 15 (9) (2003) 2549–2559.
[13] G. Biswas et al., Large-eddy simulation of High Reynolds number turbulent flow past a square cylinder, J. Eng. Mech. (ASCE) 132 (2006) 327–335.
[14] T. Igarashi, Heat transfer in separated flows, in: Proceedings of the Fifth International Heat Transfer Conference, Tokyo, 1974, pp. 300–304.
[15] T. Igarashi et al., Heat transfer in separated flows (Part1, experiments on local heat transfer from the rear of a flat plate to an air steam), Heat Transfer Jpn. Res. 4 (1) (1975) 11–32.
[16] T. Igarashi, M. Hirata, Heat transfer in separated flows (Part 3, the case of equilateral triangular prisms), Heat Transfer Jpn. Res. 6 (4) (1977) 13–39.
[17] T. Igarashi, Heat transfer in separated flows, Part 2: theoretical analysis, Heat Transfer Jpn. Res 6 (3) (1977) 60–78.
[18] T. Igarashi, Fluid flow and heat transfer in the separated region of a circular cylinder with wake control, Heat Transfer Jpn. Res. 11 (3) (1982) 1–16.
[19] T. Igarashi, Correlation between heat transfer and fluctuating pressure in separated region of a circular cylinder, Int. J. Heat Mass Transfer 27 (6) (1984) 927–937.
[20] T. Igarashi, Heat transfer from a square prism to an air stream, Int. J. Heat Mass Transfer 28 (1) (1985) 175–181.
[21] S. Aiba, H. Tsuchoda, Heat transfer around a circular cylinder near a plane boundary, Trans. JSME 51-463 (1985) 866–873.
[22] T. Igarashi, Local heat transfer from a square prism to an air stream, Int. J. Heat Mass Transfer 29 (5) (1986) 777–784.
[23] T. Igarashi, Fluid flow and heat transfer around rectangular cylinders, Int. J. Heat Mass Transfer 30 (5) (1987) 893–901.
[24] M.M. Yovanovich, G. Refai Ahmed, Experimental study of forced convection from isothermal circular and square cylinders and Toroids, J. Heat Transfer, Trans. ASME 119 (February) (1997) 70–79.
[25] A. Hossain, R.K. Brahma, Experimental investigations of fluid flow and heat transfer characteristics of a slot jet impinging on a rectangular cylinder, Warme Stoffubertragung 28 (1993) 433–439.
[26] S.J. Kline, F.A. McClintock, Describing uncertainties in single-sample experiments, Mech. Eng. 75 (1953) 3–8.